CHEMISTRY OF MATERIALS

pubs.acs.org/cm

Article

Graphene Oxide: Key to Efficient Charge Extraction and Suppression of Polaronic Transport in Hybrids with Poly (3-hexylthiophene) Nanoparticles

Eduardo Colom, Javier Hernández-Ferrer, Alejandro Galán-González, Alejandro Ansón-Casaos, Mario Navarro-Rodríguez, Elisa Palacios-Lidón, Jaime Colchero, Javier Padilla, Antonio Urbina, Raul Arenal, Ana M. Benito, and Wolfgang K. Maser*

Cite This: *Chem. Mater.* 2023, 35, 3522−3531

Read Online

ACCESS | Metrics & More | Article Recommendations | Supporting Information

ABSTRACT: Nanoparticles (NPs) of conjugated polymers in intimate contact with sheets of graphene oxide (GO) constitute a promising class of water-dispersible nanohybrid materials of increased interest for the design of sustainable and improved optoelectronic thin-film devices, revealing properties exclusively pre-established upon their liquid-phase synthesis. In this context, we report for the first time the preparation of a $P3HT_{NPs}$−GO nanohybrid employing a miniemulsion synthesis approach, whereby GO sheets dispersed in the aqueous phase serve as a surfactant. We show that this process uniquely favors a quinoid-like conformation of the P3HT chains of the resulting NPs well located onto individual GO sheets. The accompanied change in the electronic behavior of these $P3HT_{NPs}$, consistently confirmed by the photoluminescence and Raman response of the hybrid in the liquid and solid states, respectively, as well as by the properties of the surface potential of isolated individual $P3HT_{NPs}$−GO nano-objects, facilitates unprecedented charge transfer interactions between the two constituents. While the electrochemical performance of nanohybrid films is featured by fast charge transfer processes, compared to those taking place in pure $P3HT_{NPs}$ films, the loss of electrochromic effects in $P3HT_{NPs}$−GO films additionally indicates the unusual suppression of polaronic charge transport processes typically encountered in P3HT. Thus, the established interface interactions in the $P3HT_{NPs}$−GO hybrid enable a direct and highly efficient charge extraction channel via GO sheets. These findings are of relevance for the sustainable design of novel high-performance optoelectronic device structures based on water-dispersible conjugated polymer nanoparticles.

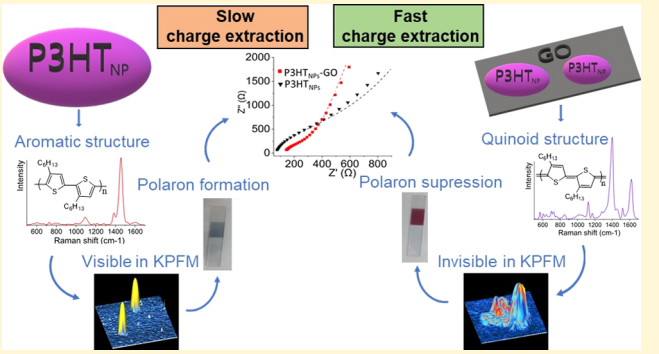

INTRODUCTION

Semiconducting π-conjugated polymers critically contribute to the development of the field of organic electronics.[1] Their tunable optical and electronic properties combined with low-cost liquid-phase processing possibilities enable the fabrication of layered optoelectronic thin-film platforms constituting the core in organic field-effect transistors (OFETs),[2] organic photovoltaics (OPV),[3] light-emitting devices (OLEDs),[4] and electrochromic applications.[5] A benchmark conjugated polymer, being used as a photoactive layer in these applications, is poly(3-hexylthiophene) (P3HT).[6] Processed into films, its polymer chains are able to crystallize, forming aggregate structures. These nanocrystalline aggregates have a significant influence on the optoelectronic, charge transfer, and charge transport properties of the resulting P3HT films.[7,8] Controlling film fabrication parameters,[9] applying thermal post-treatment steps,[10] making use of donor−acceptor blends,[11] and exploiting chemical doping[12] or electrochemical oxidation approaches[13] are widely studied strategies to influence the nanocrystalline aggregate structure and their effects on the exciton[14] and polaron dynamics[15] and to establish favorable interface interactions[16] to achieve enhanced device performance of layered film devices. More recently, self-assembly strategies shaping conjugated polymers into nanofibers or spherical nanoparticles have enjoyed increased interest.[17−21] They convey the advantage that the aggregation structure of the polymer chains in these nanoparticles is exclusively pre-established upon their formation in the liquid phase and that the resulting optoelectronic properties are not being altered

Received: January 2, 2023
Revised: April 5, 2023
Published: April 20, 2023

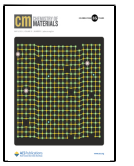

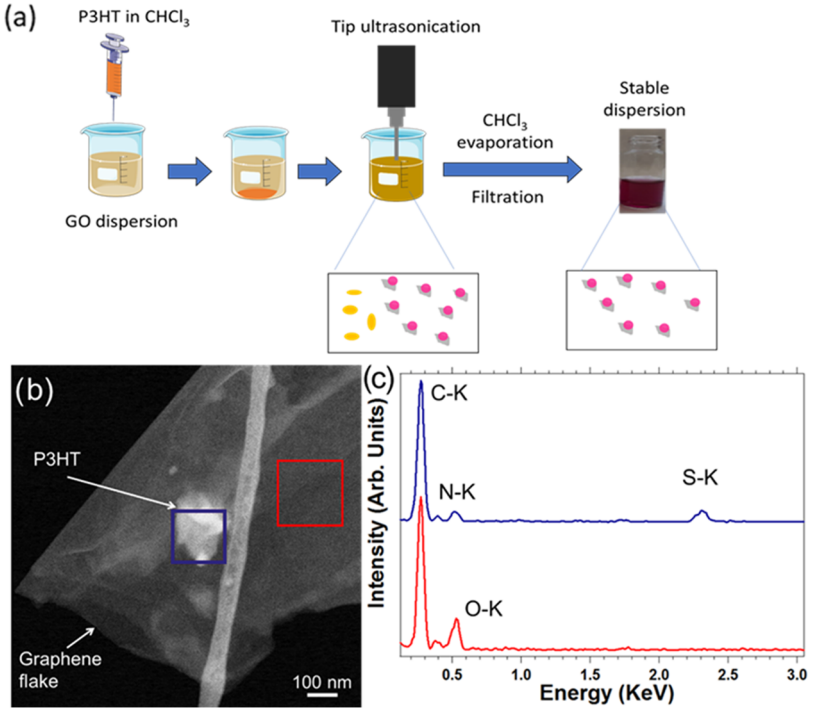

Figure 1. (a) Scheme of the employed $P3HT_{NPs}$–GO miniemulsion synthesis route. (b) HAADF-STEM image of a $P3HT_{NP}$–GO hybrid nanostructure. (c) EDS spectra of a region related to the $P3HT_{NP}$ located on GO (blue area in (b)) and of a zone related to GO alone (red area in (b)).

when processed into films, thus eliminating tedious tasks of controlling film formation parameters.[22] Moreover, the liquid phase approaches, involving either emulsion or reprecipitation technologies, provide a unique opportunity to create stable aqueous dispersions of conjugated polymer nanoparticles and environmentally friendly processing possibilities.[19] In addition, the self-assembly routes facilitate exciting pathways to interface $P3HT_{NPs}$ with different kinds of functional materials and to design novel nanohybrid materials, such as donor–acceptor core–shell nanoparticles of P3HT–PCBM[23] and P3HT–CdSe[24] or charge transfer complexes based on $P3HT_{NPs}$ and transition-metal dichalcogenides, such as $P3HT_{NPs}$–MoS_2 and $P3HT_{NPs}$–WS_2.[25] A functional platform of special interest for optoelectronic applications is the use of graphene oxide (GO).[26,27] Providing tunable conductive properties, it enables improved charge transfer properties and offers promise as a transport layer for electrons and holes in OPV devices.[28] Furthermore, being of amphiphilic character, GO suitably can be used in liquid-phase self-assembly approaches of conjugated polymers to establish improved interface interactions.[28,29] More recently, we have shown that the presence of GO sheets, used as an additive in the water phase of a reprecipitation synthesis process, uniquely favors the formation of P3HT chains with an enhanced planar conformation upon the liquid-phase self-assembly process.[30,31] This game-changing role of GO thus facilitates the enhanced development of J-aggregates inside the $P3HT_{NPs}$, being responsible for establishing close interface interactions between $P3HT_{NPs}$ located on GO sheets and the creation of a water-soluble $P3HT_{NPs}$–GO charge transfer complex with enhanced optoelectronic properties. While in situ reprecipitation processes thus successfully exploit the presence of GO sheets, the influence of GO in emulsion-based self-assembly technologies, which intrinsically require the additional presence of a stabilizing surfactant, on the growing P3HT nanoparticles and their properties needs to be explored.

In this work, we use for the first time a miniemulsion process whereby GO, due to its amphiphilic character, serves as a surfactant additive in the aqueous phase. The morphology and electronic properties of the resulting sample are probed in the liquid phase, the solid state in the form of individual objects, and as films. Transmission electron microscopy (TEM) and atomic force microscopy (AFM) studies confirm the formation of a $P3HT_{NPs}$–GO nanohybrid consisting of $P3HT_{NPs}$ in intimate contact with GO sheets. UV–vis and fluorescence spectroscopy techniques suggest important charge interface interactions between $P3HT_{NPs}$ and GO established upon the miniemulsion process, while Raman spectroscopy demonstrates significant changes in the P3HT chain conformation of $P3HT_{NPs}$ toward a quinoid-like structure in the hybrid material. Studies of the surface potential carried out by Kelvin probe force microscopy (KPFM) on isolated individual $P3HT_{NPs}$–GO nanostructures show a distinct electronic response of the surface potential of $P3HT_{NPs}$ attached to GO sheets in the hybrid compared to that of $P3HT_{NPs}$. Cyclic voltammetry and electrochemical impedance spectroscopy analyses of the nanohybrid films reveal an efficient and fast charge extraction process when compared to that of pure $P3HT_{NPs}$. The electrochromic behavior of $P3HT_{NPs}$–GO films suggests that the established interface interaction between $P3HT_{NPs}$ and GO serves as a preferred and efficient charge extraction channel, thereby suppressing the polaronic charge transport process typically encountered in $P3HT_{NPs}$. This study thus underlines the importance of the applied synthesis approach for controlling interface interaction and establishing favorable charge transport/extraction properties in hybrids of conjugated polymer nanoparticles and sheets of graphene oxide.

https://doi.org/10.1021/acs.chemmater.3c00008
Chem. Mater. 2023, 35, 3522–3531

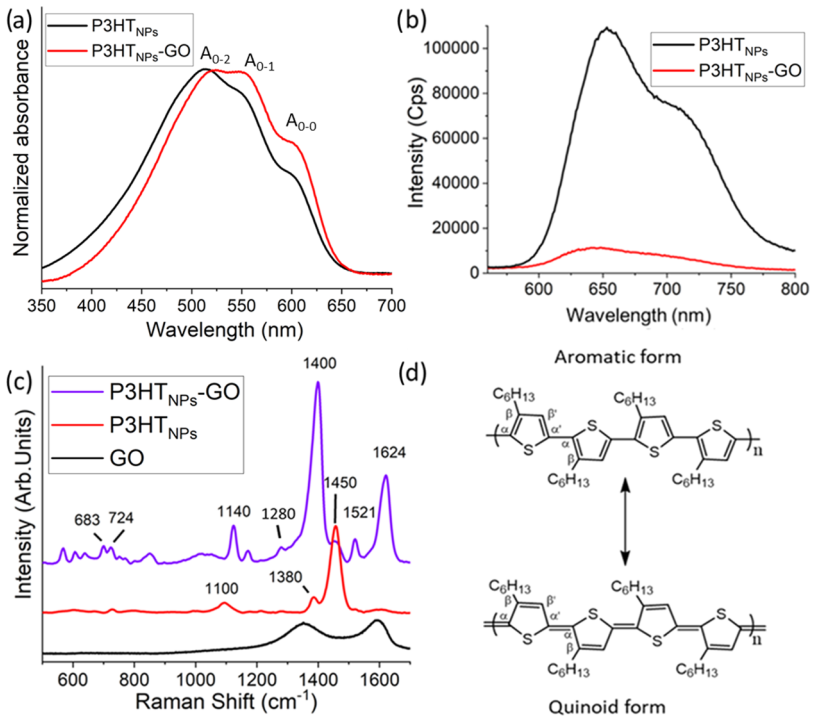

Figure 2. (a) Normalized background-corrected UV−vis absorption spectra of P3HT$_{NPs}$ and P3HT$_{NPs}$−GO. (b) Photoluminescence emission spectra of P3HT$_{NPs}$ and P3HT$_{NPs}$−GO. (c) Raman spectra of GO, P3HT$_{NPs}$, and P3HT$_{NPs}$−GO. (d) Aromatic and quinoid forms of P3HT.

RESULTS AND DISCUSSION

The P3HT$_{NPs}$−GO nanohybrid material is prepared by applying a miniemulsion synthesis approach using, for the first time, GO sheets as a surfactant in the aqueous phase. This results in stable water dispersions of the resulting P3HT$_{NP}$−GO hybrid. Figure 1a shows the scheme of the preparation approach, while the synthesis details and the critical dependence of hybrid formation on the GO sheet size are described in the Experimental Section and Supporting Information, respectively.

Transmission electron microscopy (TEM) investigations provide local information on the hybrid nanostructures, see Figure 1b,c. A GO flake of around 1 μm in size is depicted in the high-angle annular dark-field (HAADF) STEM image in Figure 1b, and a structure (brighter area) is visible in the middle of this flake. Since the intensity of these HAADF images is proportional to the density of the material and the atomic number of the elements present in the analyzed region,[32,33] it is reasonable to assume that the structure located on the GO flakes corresponds to a P3HT$_{NP}$ nanoparticle. Indeed, energy dispersive X-ray (EDS) STEM analyses performed in parallel (Figure 1c) clearly reveal the presence of sulfur in this structure (see the blue highlighted square area in Figure 1b), which is absent in the region of the pristine GO flake (see the red highlighted square area in Figure 1b). These observations thus confirm that the P3HT$_{NP}$−GO hybrid is composed of P3HT$_{NPs}$ located on GO sheets.

The liquid-phase properties provide the first insight into the electronic properties and are probed by UV−vis and photoluminescence spectroscopy. UV−vis spectra of P3HT$_{NPs}$ and P3HT$_{NPs}$−GO (Figure 2a) show a broad π−π* transition absorption band ranging from 350 to 700 nm, exhibiting a series of three well-resolved peaks at 520, 560, and 620 nm, corresponding to the fundamental vibronic A_{0-2}, A_{0-1}, and A_{0-0} transitions, indicative of the presence of excitonic coupling between the P3HT chains.[34−37] The intensity ratio between the A_{0-0} and A_{0-1} transitions, as determined from the normalized background-corrected spectra (see the Supporting Information for original data and background correction), provides important information on the internal arrangement of the polymer chains. A value of 0.55 for the case of P3HT$_{NPs}$ reveals a polymer chain structure typical for the formation of H-aggregates, whereby the P3HT chains acquire a face-to-face orientation, exhibiting interchain interactions. This ratio increases to 0.65 for the case of P3HT$_{NPs}$−GO. While this value still is indicative of the presence of H-aggregates, its enhancement, associated with a decrease in the exciton coupling constant from 40 to 30 meV (see the Supporting Information, Section S3), implies either a decrease in the interchain stacking order and/or an increase in the intrachain interactions,[34,35] being facilitated by a higher degree of planarity of the polymer chain backbone.[38] This is most likely induced by the presence of GO and provides a first hint for establishing intimate interface interactions between P3HT$_{NPs}$ and GO in the nanohybrid influencing on the electronic structure of P3HT$_{NPs}$.

In Figure 2b, the photoluminescence (PL) emission spectrum of P3HT$_{NPs}$ is characterized by two intense peaks at 650 and 710 nm. Its intensity decreases by 90% in the P3HT$_{NPs}$−GO nanohybrid. Such a significant quenching effect generally is associated with the existence of charge transfer processes between the P3HT polymer chains of the carbon nanostructure.[39] Therefore, UV−vis and PL spectroscopy techniques clearly point to the formation of a strong interaction between the polymer chains of P3HT$_{NPs}$ and GO.

To study these interactions in the hybrid material in more detail, Raman spectroscopy analyses were performed on GO, P3HT$_{NPs}$, and P3HT$_{NPs}$−GO films. The GO Raman spectrum (Figure 2c) exhibits two main broad peaks attributed to the D and G bands appearing at 1350 and 1550 cm^{-1}, respectively.[26]

https://doi.org/10.1021/acs.chemmater.3c00008
Chem. Mater. 2023, 35, 3522−3531

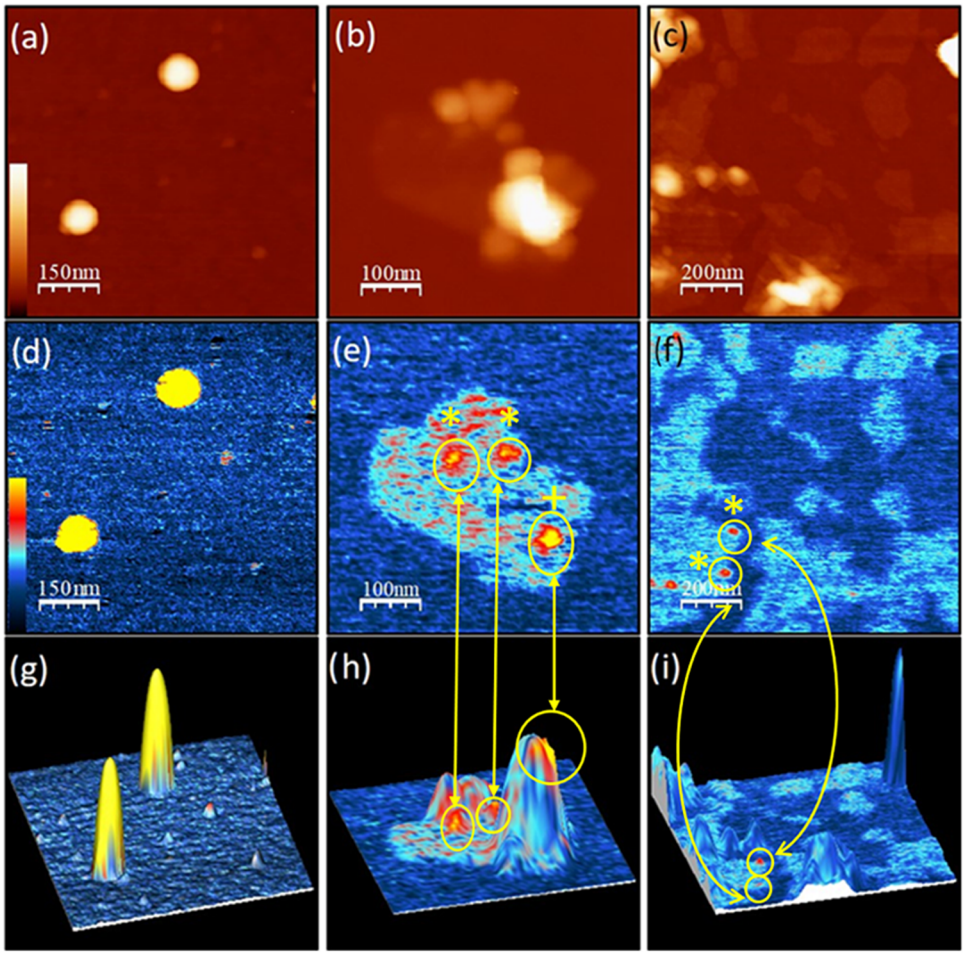

Figure 3. (a)−(c) AFM topography images: z scale = 50 nm. (d)−(f) KPFM images (z range = −50 (black) to 200 mV (yellow) with respect to the silicon substrate) of $P3HT_{NPs}$ (left column), $P3HT_{NPs}$−GO nanohybrids (middle column), and $P3HT_{NPs}$−GO nanohybrids together with pristine GO (right column) deposited on a silicon substrate. (g)−(i) Combined topographic and SP data, merged into a single 3D image such that the topographic data is represented as a 3D relief, while the SP data is superimposed as a color map. Circles marked with * and $^+$ in (e, f, h, i): zones representing high SP value and low topography (no correlation) and a zone of high SP value and high topography exhibiting a slight displacement (no direct correlation), respectively.

In the case of $P3HT_{NPs}$, the spectrum shows a typical P3HT Raman peak distribution[40] with a dominant peak located at 1450 cm^{-1}, assigned to the stretching vibrational mode of the C_α═C_β bond in the thiophene ring, a smaller peak at 1380 cm^{-1} corresponding to the stretching mode of the C_β—$C_{\beta'}$ bond, and a broad peak at 1100 cm^{-1} associated with the C—H vibrational mode[41] (Figure 2d). In contrast to these rather simple and well-known spectra, the Raman spectrum of the $P3HT_{NPs}$−GO hybrid material presents a wide number of vibrations that emerge as a result of the interactions between the polymer and GO sheets. In the lower-frequency region (<1200 cm^{-1}), several small peaks can be observed, such as those located at 724 and 683 cm^{-1}, which are related to the C_α—S—$C_{\alpha'}$ deformation, or the peaks at around 600 cm^{-1}, which are attributed to P3HT ring deformations. Additionally, the peak situated in $P3HT_{NPs}$ at 1100 cm^{-1} is shifted to 1140 cm^{-1}. Importantly, a new peak arises at 1280 cm^{-1}, which can be ascribed to the symmetric C_α═$C_{\alpha'}$ inter-ring stretching vibration.[42] This suggests an intensity redistribution of the P3HT C═C and C—C stretching modes, indicative of the existence of pronounced quinoid distortions. Moreover, in the higher-frequency region, the presence of two new sharp and intense peaks can be observed. The ones located at 1521 and 1624 cm^{-1} are usually not visible in P3HT chains and are assigned to the C_β═$C_{\beta'}$ stretching and the quinoid structure vibration, respectively.[41] Moreover, the signals typically associated with P3HT are also present, albeit their intensities and positions are uncommonly modified. In this sense, the intensity of the dominant peak at 1450 cm^{-1}, characteristic of $P3HT_{NPs}$, is noticeably less significant. Moreover, the small peak at 1380 cm^{-1} is now shifted to 1400 cm^{-1} and its intensity has notably increased. These results are in good agreement with theoretical studies carried out on sexithiophene oligomers by Mansour et al.[43] In their work, the calculated data for the vibration associated with the C_α═C_β bond in a radical cation of sexithiophene ($6T^{\bullet+}$) also exhibits a shift toward lower energies and a change in the intensities of the related peak. These findings were explained by an increased contribution of the quinoid form to the polymer structure, coinciding with the results in our $P3HT_{NPs}$−GO hybrid material. Please note that in contrast to the hybrid sample, the Raman spectrum of $P3HT_{NPs}$ simply mixed with GO does neither exhibit shifts nor new peaks, indicative of interactions between the two components (see the Supporting Information, Section 4). Therefore, the differences in the Raman spectra of the $P3HT_{NPs}$−GO hybrid and $P3HT_{NPs}$ point toward a major

https://doi.org/10.1021/acs.chemmater.3c00008
Chem. Mater. 2023, 35, 3522−3531

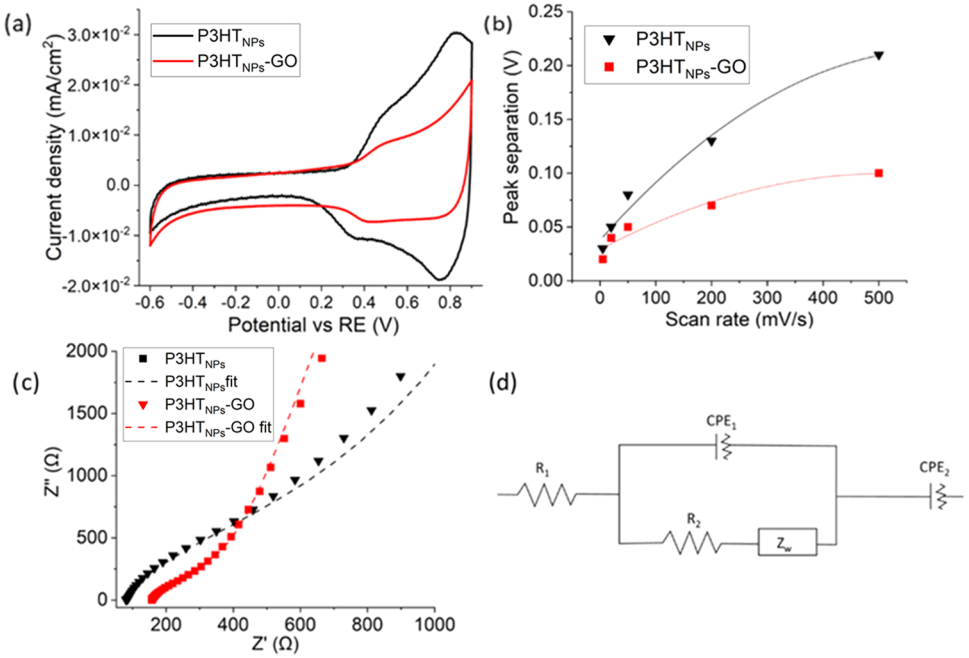

Figure 4. (a) Cyclic voltammograms of P3HT$_{NPs}$ and P3HT$_{NPs}$−GO hybrid films at a scan rate of 200 mV/s. (b) Separation of the redox peaks as a function of the scan rate for P3HT$_{NPs}$ and P3HT$_{NPs}$−GO hybrid films. (c) Nyquist plot of the impedances at 0.45 V. (d) Equivalent circuit employed to fit the impedance data.

deformation of the P3HT chains. The clear appearance of the peaks associated with the quinoid structure and the activation of vibrational modes, which are generally not observed, except under high-doping and surface-enhanced Raman spectroscopy (SERS) conditions,[41,42] reveal that the intimate interaction between P3HT$_{NPs}$ and GO is modifying the bond structure of the polymer chains from an aromatic to a quinoid conformation. Furthermore, this kind of conformational change typically has been associated with the existence of polaronic states in P3HT.[43,44]

More insight into the electronic effects caused by the structural deformations taking place in the hybrid material is obtained by combined atomic force microscopy (AFM) and Kelvin probe force microscopy (KPFM) studies probing the morphology and the surface potential (SP) of P3HT$_{NPs}$−GO nanohybrids, respectively. Samples were carefully prepared from ultradiluted dispersions drop-cast onto p-type silicon substrates (see the Experimental Section), thus ensuring to probe the nanohybrids as isolated objects. Figure 3 shows the AFM images of single, isolated P3HT$_{NPs}$ (left column), the P3HT$_{NPs}$−GO hybrid material (middle column), and the P3HT$_{NPs}$−GO hybrid material codeposited with pure GO flakes (right column). First, the morphology of the samples according to the topography images is discussed. The sample of individual P3HT$_{NPs}$ (Figure 3a) is composed of round nanoparticles exhibiting a well-defined shape with diameters and heights of about 50−100 and 20−40 nm, respectively. The negligible tip convolution for these samples suggests that the nanoparticles are flattened, most likely due to strong interactions of P3HT with the silicon substrate. The morphology of the P3HT$_{NPs}$−GO nanohybrids (Figure 3b,c) is in good agreement with the TEM observations, clearly showing that the P3HT$_{NPs}$ are located on the surface of GO flakes. The lateral size of the P3HT$_{NPs}$ on the GO flakes is about 50 nm, typically smaller than that of individual P3HT$_{NPs}$, while showing a much broader lateral size and height distribution. On smaller GO flakes, usually a single P3HT$_{NPs}$ is found (see the Supporting Information), whereas on larger GO flakes, the density of P3HT$_{NPs}$ is quite high, eventually forming aggregates. Importantly, no isolated P3HT$_{NPs}$ are observed on the sample, implying that the P3HT nanoparticles are attached quite strongly to GO as a consequence of the applied miniemulsion process.

The KPFM images (Figure 3d−f) show the surface potential (SP) of the corresponding samples, more precisely, the local difference of the Fermi Level with respect to the tip used for imaging, whereby more positive KPFM values (brighter image colors) correspond to more positively charged regions, as explained in detail in the supporting information of a previous publication.[31] To simplify data interpretation and the discussion, in the following, all SP values are given with respect to the silicon substrate, serving as an internal standard in this work. The KPFM images of isolated P3HT$_{NPs}$ (Figure 3d) show an excellent correlation of topography and surface potential, exhibiting an SP difference of +350 ± 50 mV for P3HT$_{NPs}$. By contrast, the KPFM measurements of the P3HT$_{NPs}$−GO nanohybrids (Figure 3e,f) reveal a notably distinct response. First, only a few of the P3HT$_{NPs}$−GO nanohybrids show a clear SP difference as compared to the mean SP value of GO flakes (ΔSP_{GO} = +50 ± 20 mV, light blue color), while most of the nanoparticles exhibit essentially the same SP as GO. Second, for those few nanoparticles that display a clear SP difference with respect to GO, their highest values do not surpass +150 mV (for detailed profiles, see Figure S5 in the Supporting Information). The different behavior is seen particularly well in the combined 3D representation of topography and surface potential (Figure 3g−i), which allows a precise colocalization of topographic and surface potential data. Importantly, these images show that surface potential values are not directly correlated with surface morphology. In particular, high surface potential (red-yellow color) is not always associated with the highest topographic

https://doi.org/10.1021/acs.chemmater.3c00008
Chem. Mater. 2023, 35, 3522−3531

Table 1. Fitted EIS Parameters (R, Y_0(CPEs and Z_W), α_1(CPEs)) According to the Equivalent Circuit in Figure 4d, Whereby Y_0 Expresses the Admittance Value and α is the Capacitance Degree of the CPEs

	R_1 (Ω)	R_2 (Ω)	Y_0(CPE$_1$) (S)	α_1(CPE$_1$)	Y_0(Z_w) (S)	Y_0(CPE$_2$) (S)	α_2(CPE$_2$)
P3HT$_{NPs}$	82.1	782	3.4×10^{-5}	0.88	3.2×10^{-4}	7.9×10^{-5}	1
P3HT$_{NPs}$-GO	156.3	210.4	3.7×10^{-5}	0.84	1.2×10^{-3}	4.2×10^{-5}	0.94

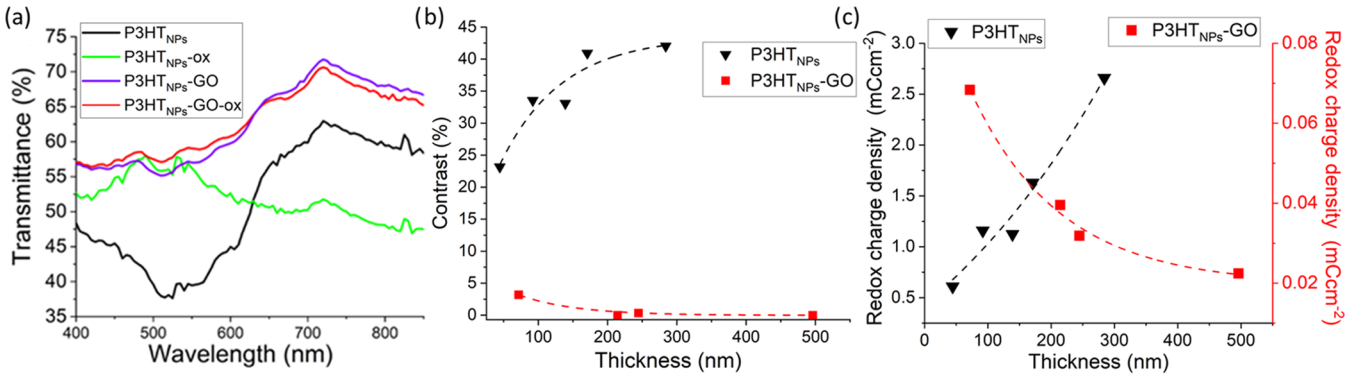

Figure 5. Electrochromic studies. (a) UV−vis transmittance spectra of P3HT$_{NPs}$ and P3HT$_{NPs}$−GO films with similar thicknesses in neutral and oxidized states. (b) Variation of the contrast as a function of the film thickness. (c) Redox charge density of the films as a function of the film thickness.

regions of the P3HT$_{NPs}$ on the GO flake, as clearly indicated by the circles in the image. Even more intriguing, some regions showing P3HT$_{NPs}$ located on GO display essentially the same SP as GO. This is especially evident in the sample composed of pure GO flakes codeposited with the P3HT$_{NPs}$−GO nanohybrids (Figure 3i). On this sample, the same SP is measured on (a) pristine GO (which can be considered a local "reference potential for GO"), (b) on the part of the isolated nanohybrid not covered by P3HT$_{NPs}$, and (c) most parts of the isolated nanohybrid covered by P3HT$_{NPs}$. It thus appears that most of the P3HT$_{NPs}$ located on the GO flakes in the hybrid sample are transparent in the KPFM images. Since this facilitates only the observation of the surface potential of the underneath GO sheet, it suggests a lack of free charge carriers in the P3HT$_{NPs}$ of the hybrid material. This rather complex electronic behavior of the nanohybrids implies that the P3HT$_{NPs}$ are not simply adsorbed onto the GO sheets but experience a strong interaction involving the modification of their electronic structure. Most likely, this is related to the enhanced stabilization of the quinoid chain conformation of the P3HTN$_{NPs}$ on GO, as implied by the Raman results, being established upon the in situ miniemulsion process.

To determine the implications of the distinct electronic behavior, electrochemical studies were carried out on P3HT$_{NPs}$ and P3HT$_{NPs}$−GO films. Cyclic voltammetry (CV) experiments performed on P3HT and P3HT−GO films are shown in Figure 4a. The voltammogram displays two oxidation peaks centered at 0.45 and 0.8 V, ascribed to aggregated and amorphous zones of the P3HT, respectively.[45] The peak centered at 0.45 V is of special interest since p-doping processes of P3HT take place during this oxidation wave and are usually described as the key processes that enable the formation of the polaronic states of P3HT.[13] As observed in the cyclic voltammograms, the behavior of this oxidation peak at 0.45 V is different in the case of P3HT$_{NPs}$ and the P3HT−GO hybrid. Cyclic voltammetry measurements at different scan rates were performed on P3HT$_{NPs}$ and P3HT$_{NPs}$−GO films (see SI Figure S6a,b) to assess the evolution of the associated redox peaks and thus the kinetic reversibility of the charge transfer processes. It is noticed that the shift of the oxidation and reduction peaks in P3HT$_{NPs}$ films are significantly larger than in P3HT−GO films for the same scan rates (Figure 4b). While the former behavior points to irreversible processes and rather slow electron transfer rates in P3HT$_{NPs}$ films, the scan-rate-independent potential difference for the P3HT$_{NPs}$−GO hybrid films indicates a more Nernstian behavior, enabling a fast electron transfer between the film and the electrolyte solution.[46−48] The existence of faster charge transfer processes in the P3HT$_{NPs}$−GO hybrid film can be related to the modulation of the P3HT structure caused by the interaction with the GO sheets, in full agreement with the Raman and KPFM observations.

These phenomena were further explored by electronic impedance spectroscopy (EIS) studies, which were carried out at 0.45 V, the oxidation point of P3HT. The noticeable changes in the Nyquist plot (Figure 4c) of both types of materials underline the existence of different electronic processes in the films. The model employed to fit the experimental data (Figure 4d) was developed following a previous work of our group with similar hybrid compounds.[49] The equivalent circuit consists of resistance R_1 in series with a parallel combination of constant-phase element CPE$_1$ (an element used to describe a nonideal capacitor) and resistance R_2 in series with a Warburg impedance, which refers to a finite-length diffusion effect in the film (Z_w).[49] Finally, a second CPE (CPE$_2$) is placed in series with the previous elements. The parameters employed in the equivalent circuit are related to different elements of the electronic system. Thus, resistance R_1 is associated with a resistance inherent to the measurement system (which includes both the electrolyte and electrode). CPE$_1$ is associated with the capacitance of the film−electrolyte interface, while R_2 is assigned to the resistance of the charge transfer processes between the film and the electrolyte. The Warburg impedance is attributed to the diffusion of the charged species in the inner part of the film and along the interface between the film and solution, being necessary to equilibrate the charge generated at the electrode. CPE$_2$ is an element that refers to the intrinsic electrochemical capacitance

https://doi.org/10.1021/acs.chemmater.3c00008
Chem. Mater. 2023, 35, 3522−3531

of the film. The fitting results (Table 1) reveal that both R_2 and Z_W are three times lower in the P3HT$_{NPs}$−GO hybrid films compared to the ones in P3HT$_{NPs}$. This clearly underlines the formation of favorable charge transfer processes between P3HT$_{NPs}$ and GO sheets in the hybrid films. This is also in agreement with the decrease of the CPE_2 value, suggesting that less charge is stored in the P3HT$_{NPs}$ of the hybrid films, as consistently observed in the cyclic voltammogram in Figure 4a, and in full agreement with the KPFM results.

As stated above, the oxidation processes occurring at positive potentials are typically associated with the appearance of the polaronic states in the polymer. When P3HT is exposed to potentials higher than 0.45 V (vs Ag/AgCl), it undergoes a p-doping process, which entails the formation of positively charged polymer chains and the change in the main conformation in the bond structure along the P3HT to a more quinoid-like form (Figure 2d).[50] All of these conformational and electronic alterations usually induce polaronic states, noticed as bands in the NIR appearing on the cost of those in the UV−vis range.[50] This effect forms the base for electrochromic applications in P3HT-based materials.[50] We thus carried out electrochromic studies to further analyze the charge transport behavior in our P3HT$_{NPs}$−GO hybrid material.

The transmittance spectra of the two types of films in their neutral and oxidized states (Figure 5a) reveal a clear change of the peak at 510 nm, indicating the transition from the neutral to the oxidized state (between 0 and 0.6 V) in P3HT$_{NPs}$. The former (neutral state) tends to absorb in the visible range of the spectra, while the latter (oxidized state) presents its transitions in the NIR.[51] In contrast, in the P3HT−GO hybrid, the transmittance spectrum remains almost constant even after the oxidation process.

The electrochromic performance of the films of both materials is evaluated at λ_{max} = 510 nm (the wavelength corresponding to the maximum transmittance modulation), providing the contrast (transmittance variation between neutral and oxidized states) as a function of the film thickness (Figure 5b). Two distinct tendencies can be observed for the P3HT$_{NPs}$ and the P3HT−GO hybrid. In the case of P3HT$_{NP}$, the change in transmittance at 510 nm between neutral and oxidized states increases with the thickness of the film until a maximum is reached (in this case, for a film of ∼300 nm), as typically observed in conductive polymeric systems.[51−53] However, in the case of the P3HT$_{NPs}$−GO hybrid, the electrochromic response is almost negligible, even for the thicker films. This unexpected observation is in sharp contrast to previous studies on the influence of GO on the electrochromic effects of P3HT.[54] A directly related observation refers to the thickness-dependent charge density of the films. While P3HT$_{NPs}$ films show an enhancement of charge density with increased film thickness, typical for conductive polymers, the P3HT$_{NPs}$−GO nanohybrid exhibits the opposite behavior, offering advantages when prepared as very thin films (Figure 5c). Additionally, the observation that redox charge densities for P3HT$_{NPs}$−GO films are two orders of magnitude lower compared to those obtained in P3HT$_{NPs}$ films confirms a notable loss in redox activity, as previously mentioned. Therefore, the unexpected loss of electrochromic effects in the P3HT$_{NPs}$−GO hybrid films combined with the unusual thickness dependence indicates the suppression of the characteristic polaronic charge transport process in the nanohybrid films, associated with the established P3HT$_{NPs}$−GO interface interactions favored by the more planar quinoid conformation of the polymer chains in the P3HT$_{NPs}$ upon their formation in the miniemulsion process.

CONCLUSIONS

In this study, we report on the formation of a P3HT$_{NPs}$−GO nanohybrid through a miniemulsion process employing GO as a surfactant. We demonstrate that the presence of GO in this process favors the formation of a quinoid conformation of the P3HT polymer chains, enabling an intimate contact of the P3HT$_{NPs}$ to the underlying GO sheets. Our studies in the liquid phase, on individual objects and on supported films, consistently reveal that the established interface interaction between P3HT$_{NP}$ and GO facilitates an effective channel to extract charges from the P3HT$_{NPs}$ in the hybrid material, thereby suppressing the polaronic charge transport processes in the polymer chains of the P3HT$_{NP}$ in the nanohybrid. This unprecedented finding underlines the importance of the applied synthesis approach for controlling interface interactions and establishing favorable charge transport/extraction properties in hybrids of conjugated polymer nanoparticles and sheets of graphene oxide. It further constitutes an important fundamental contribution toward an enhanced understanding of nonpolaronic transport phenomena, a topic of very recent interest in the field of conducting polymers.[55,56] Moreover, the possibility of achieving effective and rapid charge extraction from P3HT$_{NPs}$ let us envisage the sustainable design of novel high-performance optoelectronic device structures based on water-dispersible conjugated polymer nanoparticles.

EXPERIMENTAL SECTION

Materials. Regio-regular poly(3-hexylthiophene) with 95% RR and MW > 5000, $CHCl_3$, and THF were purchased from Sigma-Aldrich.

Synthesis. For the synthesis of the P3HT$_{NPs}$−GO hybrid, P3HT was dissolved in $CHCl_3$ (1 mg/mL) and stirred for 20 min. Then, 1 mL of the solution was transferred to 10 mL of water solution containing 1 mg of the desired GO dispersion. The solution was tip-sonicated for 2 min at maximum power (400 W, 24 kHz as the maximum frequency) until it turned into a brown dispersion. Then, the emulsion was heated to 65 °C under vigorous stirring until chloroform was removed and the solution transformed into a transparent purple dispersion. Finally, the as-prepared dispersions were filtrated to remove nondispersed polymer excess. Dispersions obtained with different GO flake sizes were studied (see the S.I., Figure S2), and the most stables were found to be those made with the smallest GO flake dispersion (4 h) consistently employed in this work. P3HT$_{NPs}$ nanoparticles as the control sample was prepared by the reprecipitation process. P3HT was dissolved 1 mg/mL in tetrahydrofuran (THF) and stirred overnight. Thereafter, the solution was mildly heated at 35 °C until the color changed to bright orange. Then, 1 mL of P3HT solution was rapidly injected into 10 mL of deionized water. Obtained dispersions were mildly heated until THF was removed from the solution and the solution remained stable.

Characterization. For TEM/EDS characterization, original dispersions of the P3HT materials were diluted to a 1:100 proportion and then drop-cast onto lacey carbon TEM grids. TEM and EDS characterizations were performed on a probe-corrected Thermo Fisher Titan-Low-Base 60-300 operating at 300 kV (equipped with a Cs-probe corrector (CESCOR from CEOS GmbH)). EDS data were recorded using an Oxford Instruments Ultim Max TLE 100 spectrometer.

UV−Vis absorption spectra of dispersions were recorded on a Shimadzu UV-2401 PC spectrophotometer. The concentration of the water dispersions was adjusted to acquire an absorbance value of 0.3 at 510 nm. Photoluminescence (PL) emission spectra were recorded on a Horiba Jobin Yvon Fluoromax-P using an absorption wavelength

https://doi.org/10.1021/acs.chemmater.3c00008
Chem. Mater. 2023, 35, 3522−3531

of 510 nm, employing dispersions used in UV−vis spectroscopy using a 10 mm pathlength quartz cuvette.

Samples for PL were measured from the same dispersions with an absorbance value of 0.3 at 510 nm in UV−vis. For Raman analysis, dispersions in water of $P3HT_{NP}$, P3HT−GO, and GO were deposited onto glass substrates by spray coating and measured by Raman spectroscopy using an excitation wavelength of 532 nm by a Horiba Jobin Yvon HRLAB HR 800 UV apparatus.

AFM/KPFM samples were prepared by drop casting of ultradiluted solutions (1:100 with respect to the original solution) of both $P3HT_{NPs}$ and $P3HT_{NPs}$−GO on highly doped p-type silicon (1−10 Ω·cm, Siltronix). Prior to deposition, the surface was cleaned with ethanol to remove organic contaminants and then rinsed with double distilled water; afterward, the surface was exposed to an ozone atmosphere to make the substrate hydrophilic. Directly after deposition, the samples were again rinsed with double distilled water and then mildly heated (between 40 and 50 °C) for about 30 min to evaporate physisorbed water. The measurements were performed with Pt-coated tips (OMCL-AC240TM-R3, k = 2 N/m) mounted on a Nanotec SFM system provided with a PLL/dynamic board under ambient conditions (RH = 45%, T = 25 °C). The topography images were acquired in the amplitude modulation noncontact dynamic mode (AM-DSFM) with an oscillation amplitude of 10 nm and a tip−sample distance between 7 and 10 nm. The KPFM images were acquired in the frequency modulation mode (FM-KPFM) with V_{AC} = 500 mV and a frequency ν_{AC} = 7 kHz. The silicon substrate, probed by the Pt tip, revealed a surface potential of +600 mV. To simplify the discussion, the surface potential values of the nano-objects deposited on the silicon substrates were always provided with respect to the silicon substrate, serving as an internal reference standard in this work.

Electrochemical experiments were performed with an AUTOLAB PGSTAT302N potentiostat. Cyclic voltammetry studies of the hybrids are carried out under nitrogen in a three-electrode cell using 0.1 M $NaClO_4$ in dry acetonitrile as a supporting electrolyte. The samples were spray-coated onto FTO glasses and used as working electrodes. Carbon and silver/silver chloride (Ag/AgCl, calibrated at 0.19 V vs NHE) were employed as counter and reference electrodes, respectively. EIS experiments were carried out over the same samples in the 0.1−10^6 Hz frequency range.

To study their electrochromic properties, aqueous dispersion of $P3HT_{NPs}$−GO and $P3HT_{NPs}$ were used to obtain 4−5 films of increasing thicknesses in each case. Film thicknesses were measured with a Dektak 50 profilometer. Films were deposited via spray coating employing an Iwata Eclipse HP-BC airbrush with nitrogen as the carrier gas (∼0.8 bar) onto heated (120 °C) indium tin oxide (ITO)/glass (8−12 Ω/sq., 7 mm × 50 mm × 0.7 mm, Delta Technologies Ltd.).

Spectroelectrochemical measurements were performed in a three-electrode cell with 0.1 M $LiClO_4$ (ACN) as an electrolyte (with Pt wire as a counter electrode and an Ag/AgCl wire as a reference electrode, calibrated at 0.19 V vs NHE) using a Varian Cary 50 UV−Vis spectrophotometer and a BioLogic SP-50 potentiostat. Cyclic voltammetry was also performed (−0.4 to 1.1 V vs Ag/AgCl wire, 50 mV/s). Charge density values of the films were obtained from the integration of the CV curves. Stationary spectra in the visible range were obtained at neutral and oxidized states, and transmittance values at 510 nm were extracted from these spectra.

■ ASSOCIATED CONTENT

Supporting Information

The Supporting Information is available free of charge at https://pubs.acs.org/doi/10.1021/acs.chemmater.3c00008.

Additional information on the synthesis of graphene oxide, stability of water dispersions of $P3HT_{NPs}$−GO using different GO sheet sizes, UV−vis and Raman spectra, AFM/KPFM images of $P3HT_{NPs}$ and P3HT−GO nanohybrids, and cyclic voltammetry results of films of $P3HT_{NPs}$ and $P3HT_{NPs}$−GO as a function of the scan rate (PDF)

■ AUTHOR INFORMATION

Corresponding Author

Wolfgang K. Maser − *Instituto de Carboquímica (ICB-CSIC), E-50011 Zaragoza, Spain;* orcid.org/0000-0003-4253-0758; Email: wmaser@icb.csic.es

Authors

Eduardo Colom − *Instituto de Carboquímica (ICB-CSIC), E-50011 Zaragoza, Spain*

Javier Hernández-Ferrer − *Instituto de Carboquímica (ICB-CSIC), E-50011 Zaragoza, Spain;* orcid.org/0000-0002-6586-6935

Alejandro Galán-González − *Instituto de Carboquímica (ICB-CSIC), E-50011 Zaragoza, Spain; Centro de Investigaciones Científicas Avanzadas, Universidade da Coruña (CICA), E-15008 San Vicenzo de Elviña, A Coruña, Spain*

Alejandro Ansón-Casaos − *Instituto de Carboquímica (ICB-CSIC), E-50011 Zaragoza, Spain;* orcid.org/0000-0002-3134-8566

Mario Navarro-Rodríguez − *Departamento de Física, Edificio CIOyN, Universidad de Murcia, E-30100 Murcia, Spain;* orcid.org/0000-0001-7676-6609

Elisa Palacios-Lidón − *Departamento de Física, Edificio CIOyN, Universidad de Murcia, E-30100 Murcia, Spain;* orcid.org/0000-0002-0785-8566

Jaime Colchero − *Departamento de Física, Edificio CIOyN, Universidad de Murcia, E-30100 Murcia, Spain;* orcid.org/0000-0003-0887-4549

Javier Padilla − *Departamento de Física Aplicada y Tec. Naval, Universidad Politécnica de Cartagena, E-30202 Cartagena, Spain;* orcid.org/0000-0002-9974-7774

Antonio Urbina − *Departamento de Ciencias e Instituto de Materiales Avanzados y Matemáticas (INAMAT²), Universidad Pública de Navarra (UPNA), E-31006 Pamplona, Spain; Laboratorio de Microscopias Avanzadas (LMA), Universidad de Zaragoza, E-50018 Zaragoza, Spain;* orcid.org/0000-0002-3961-1007

Raul Arenal − *Instituto de Nanociencia y Materiales de Aragón (INMA-CSIC-Univ. Zaragoza), E-50009 Zaragoza, Spain; ARAID Foundation, E-50018 Zaragoza, Spain;* orcid.org/0000-0002-2071-9093

Ana M. Benito − *Instituto de Carboquímica (ICB-CSIC), E-50011 Zaragoza, Spain;* orcid.org/0000-0002-8654-7386

Complete contact information is available at: https://pubs.acs.org/10.1021/acs.chemmater.3c00008

Author Contributions

The manuscript was written through the contribution of all authors. All authors have given approval to the final version of the manuscript.

Notes

The authors declare no competing financial interest.

■ ACKNOWLEDGMENTS

This work was funded by Spanish MCIN/AEI/10.13039/501100011033 under projects PID2019-104272RB-C51, PID2019-104272RB-C52, PID2019-104272RB-C55, and

PID2019-104739GB-100. Financial support from Gobierno de Aragon (DGA) under project "Grupos Consolidados" T03_20R is acknowledged. E.C. is grateful for PhD grant BES2017-080020 funded by MCIN/AEI/10.13039/501100011033 and by "ESF Investing in your future". M.N.R.'s work was financed by grant PID2019-104272RB-C52/PRE2020-094503 funded by MCIN/AEI/10.13039/501100011033 and by "'ESF Investing in your future"'. R.A. acknowledges support from EU H2020 "ESTEEM3" (Grant number 823717) and Graphene Flagship (881603). TEM studies were performed in the Laboratorio de Microscopias Avanzadas (LMA), Universidad de Zaragoza (Spain).

REFERENCES

(1) Reynolds, J. R.; Thompson, B. C.; Skotheim, T. A. *Conjugated Polymers: Properties, Processing, and Applications (Handbook of Conducting Polymers)*, 4th ed.; CRC Press, 2019.
(2) Sirringhaus, H. 25th Anniversary Article: Organic Field-Effect Transistors: The Path Beyond. *Adv. Mater.* **2014**, *26*, 1319−1335.
(3) Heeger, A. J. 25th Anniversary Article: Bulk Heterojunction Solar Cells: Understanding the Mechanism of Operation. *Adv. Mater.* **2014**, *26*, 10−28.
(4) Walzer, K.; Männig, B.; Pfeiffer, M.; Leo, K. Highly Efficient Organic Devices Based on Electrically Doped Transport Layers. *Chem. Rev.* **2007**, *107*, 1233−1271.
(5) Beaujuge, P. M.; Reynolds, J. R. Color Control in π-Conjugated Organic Polymers for Use in Electrochromic Devices. *Chem. Rev.* **2010**, *110*, 268−320.
(6) Tremel, K.; Ludwigs, S. Morphology of P3HT in Thin Films in Relation to Optical and Electrical Properties. In *P3HT Revisited − From Molecular Scale to Solar Cell Devices*, 1st ed.; Ludwigs, S., Ed.; Springer, 2014; Vol. *265*, pp 39−82.
(7) Reid, O. G.; Nekuda Malik, J. A.; Latini, G.; Dayal, S.; Kopidakis, N.; Silva, C.; Stingelin, N.; Rumbles, G. The Influence of Solid-state Microstructure on the Origin and Yield of Long-lived Photogenerated Charge in Neat Semiconducting Polymers. *J. Polym. Sci., Part B: Polym. Phys.* **2012**, *50*, 27−37.
(8) Paquin, F.; Rivnay, J.; Salleo, A.; Stingelin, N.; Silva-Acuña, C. Multi-Phase Microstructures Drive Exciton Dissociation in Neat Semicrystalline Polymeric Semiconductors. *J. Mater. Chem. C* **2015**, *3*, 10715−10722.
(9) Helgesen, M.; Søndergaard, R.; Krebs, F. C. Advanced Materials and Processes for Polymer Solar Cell Devices. *J. Mater. Chem.* **2010**, *20*, 36−60.
(10) Padinger, F.; Rittberger, R. S.; Sariciftci, N. S. Effects of Postproduction Treatment on Plastic Solar Cells. *Adv. Funct. Mater.* **2003**, *13*, 85−88.
(11) Baran, D.; Ashraf, R. S.; Hanifi, D. A.; Abdelsamie, M.; Gasparini, N.; Röhr, J. A.; Holliday, S.; Wadsworth, A.; Lockett, S.; Neophytou, M.; Emmott, C. J. M.; Nelson, J.; Brabec, C. J.; Amassian, A.; Salleo, A.; Kirchartz, T.; Durrant, J. R.; McCulloch, I. Reducing the Efficiency-Stability-Cost Gap of Organic Photovoltaics with Highly Efficient and Stable Small Molecule Acceptor Ternary Solar Cells. *Nat. Mater.* **2017**, *16*, 363−369.
(12) Salzmann, I.; Heimel, G.; Oehzelt, M.; Winkler, S.; Koch, N. Molecular Electrical Doping of Organic Semiconductors: Fundamental Mechanisms and Emerging Dopant Design Rules. *Acc. Chem. Res.* **2016**, *49*, 370−378.
(13) Neusser, D.; Malacrida, C.; Kern, M.; Gross, Y. M.; Van Slageren, J.; Ludwigs, S. High Conductivities of Disordered P3HT Films by an Electrochemical Doping Strategy. *Chem. Mater.* **2020**, *32*, 6003−6013.
(14) Osterloh, F. E.; Holmes, M. A.; Chang, L.; Moulé, A. J.; Zhao, J. Photochemical Charge Separation in Poly(3-Hexylthiophene) (P3HT) Films Observed with Surface Photovoltage Spectroscopy. *J. Phys. Chem. C* **2013**, *117*, 26905−26913.
(15) Park, K. H.; Son, S. Y.; Kim, J. O.; Kang, G.; Park, T.; Kim, D. Role of Disorder in the Extent of Interchain Delocalization and Polaron Generation in Polythiophene Crystalline Domains. *J. Phys. Chem. Lett.* **2018**, *9*, 3173−3180.
(16) Tsoi, W. C.; Spencer, S. J.; Yang, L.; Ballantyne, A. M.; Nicholson, P. G.; Turnbull, A.; Shard, A. G.; Murphy, C. E.; Bradley, D. D. C.; Nelson, J.; Kim, J. S. Effect of Crystallization on the Electronic Energy Levels and Thin Film Morphology of P3HT:PCBM Blends. *Macromolecules* **2011**, *44*, 2944−2952.
(17) Tuncel, D.; Demir, H. V. Conjugated Polymer Nanoparticles. *Nanoscale* **2010**, *2*, 484−494.
(18) Pecher, J.; Mecking, S. Nanoparticles of Conjugated Polymers. *Chem. Rev.* **2010**, *110*, 6260−6279.
(19) Holmes, A.; Deniau, E.; Lartigau-Dagron, C.; Bousquet, A.; Chambon, S.; Holmes, N. P. Review of Waterborne Organic Semiconductor Colloids for Photovoltaics. *ACS Nano* **2021**, *15*, 3927−3959.
(20) MacFarlane, L. R.; Shaikh, H.; Garcia-Hernandez, J. D.; Vespa, M.; Fukui, T.; Manners, I. Functional Nanoparticles through π-Conjugated Polymer Self-Assembly. *Nat. Rev. Mater.* **2021**, *6*, 7−26.
(21) Kang, S.; Yoon, T. W.; Kim, G.; Kang, B. Review of Conjugated Polymer Nanoparticles: From Formulation to Applications. *ACS Appl. Nano Mater.* **2022**, *5*, 17436−17460.
(22) Baghgar, M.; Barnes, M. D. Work Function Modification in P3HT H/J Aggregate Nanostructures Revealed by Kelvin Probe Force Microscopy and Photoluminescence Imaging. *ACS Nano* **2015**, *9*, 7105−7112.
(23) Palacio Valera, A.; Schatz, C.; Ibarboure, E.; Kubo, T.; Segawa, H.; Chambon, S. Elaboration of PCBM Coated P3HT Nanoparticles: Understanding the Shell Formation. *Front. Energy Res.* **2019**, *6*, 146.
(24) Istif, E.; Kagkoura, A.; Hernandez-Ferrer, J.; Stergiou, A.; Skaltsas, T.; Arenal, R.; Benito, A. M.; Maser, W. K.; Tagmatarchis, N. Self-Assembled Core-Shell CdTe/Poly(3-Hexylthiophene) Nanoensembles as Novel Donor-Acceptor Light-Harvesting Systems. *ACS Appl. Mater. Interfaces* **2017**, *9*, 44695−44703.
(25) Canton-Vitoria, R.; Istif, E.; Hernández-Ferrer, J.; Urriolabeitía, E.; Benito, A. M.; Maser, W. K.; Tagmatarchis, N. Integrating Water-Soluble Polythiophene with Transition-Metal Dichalcogenides for Managing Photoinduced Processes. *ACS Appl. Mater. Interfaces* **2019**, *11*, 5947−5956.
(26) Eda, G.; Chhowalla, M. Chemically Derived Graphene Oxide: Towards Large-Area Thin-Film Electronics and Optoelectronics. *Adv. Mater.* **2010**, *22*, 2392−2415.
(27) Loh, K. P.; Bao, Q.; Eda, G.; Chhowalla, M.; et al. Graphene Oxide as a Chemically Tunable Platform for Optical Applications. *Nat. Chem.* **2010**, *2*, 1015−1024.
(28) Liu, J.; Durstock, M.; Dai, L. Graphene Oxide Derivatives as Hole- and Electron-Extraction Layers for High-Performance Polymer Solar Cells. *Energy Environ. Sci.* **2014**, *7*, 1297−1306.
(29) Vallés, C.; Jiménez, P.; Muñoz, E.; Benito, A. M.; Maser, W. K. Simultaneous Reduction of Graphene Oxide and Polyaniline: Doping-Assisted Formation of a Solid-State Charge-Transfer Complex. *J. Phys. Chem. C* **2011**, *115*, 10468−10474.
(30) Istif, E.; Hernández-Ferrer, J.; Urriolabeitia, E. P.; Stergiou, A.; Tagmatarchis, N.; Fratta, G.; Large, M. J.; Dalton, A. B.; Benito, A. M.; Maser, W. K. Conjugated Polymer Nanoparticle−Graphene Oxide Charge-Transfer Complexes. *Adv. Funct. Mater.* **2018**, *28*, No. 1707548.
(31) Palacios-Lidón, E.; Istif, E.; Benito, A. M.; Maser, W. K.; Colchero, J. Nanoscale J-Aggregates of Poly(3-Hexylthiophene): Key to Electronic Interface Interactions with Graphene Oxide as Revealed by KPFM. *Nanoscale* **2019**, *11*, 11202−11208.
(32) Pennycook, S. J.; Nellist, P. D. *Scanning Transmission Electron Microscopy - Imaging and Analysis*; Springer, 2011.
(33) Liu, L.; Díaz, U.; Arenal, R.; Agostini, G.; Concepción, P.; Corma, A. Generation of Subnanometric Platinum with High Stability during Transformation of a 2D Zeolite into 3D. *Nat. Mater.* **2017**, *16*, 132−138.
(34) Clark, J.; Silva, C.; Friend, R. H.; Spano, F. C. Role of Intermolecular Coupling in the Photophysics of Disordered Organic

Semiconductors: Aggregate Emission in Regioregular Polythiophene. *Phys. Rev. Lett.* **2007**, *98*, No. 206406.
(35) Clark, J.; Chang, J. F.; Spano, F. C.; Friend, R. H.; Silva, C. Determining Exciton Bandwidth and Film Microstructure in Polythiophene Films Using Linear Absorption Spectroscopy. *Appl. Phys. Lett.* **2009**, *94*, 163306.
(36) Ghosh, R.; Spano, F. C. Excitons and Polarons in Organic Materials. *Acc. Chem. Res.* **2020**, *53*, 2201−2211.
(37) Spano, F. C.; Silva, C. H- and J-Aggregate Behavior in Polymeric Semiconductors. *Annu. Rev. Phys. Chem.* **2014**, *65*, 477−500.
(38) Nagarjuna, G.; Baghgar, M.; Labastide, J. A.; Algaier, D. D.; Barnes, M. D.; Venkataraman, D. Tuning Aggregation of Poly-(3-Hexylthiophene) within Nanoparticles. *ACS Nano* **2012**, *6*, 10750−10758.
(39) Hill, C. M.; Zhu, Y.; Pan, S. Fluorescence and Electroluminescence Quenching Evidence of Interfacial Charge Transfer in Poly (3-Hexylthiophene): Graphene Oxide Bulk Heterojunction Photovoltaic Devices. *ACS Nano* **2011**, *5*, 942−951.
(40) Louarn, G.; Trznadel, M.; Buisson, J. P.; Laska, J.; Pron, A.; Lapkowski, M.; Lefrant, S. Raman Spectroscopic Studies of Regioregular Poly(3-Alkylthiophenes. *J. Phys. Chem. A* **1996**, *100*, 12532−12539.
(41) Baibarac, M.; Lapkowski, M.; Pron, A.; Lefrant, S.; Baltog, I. SERS Spectra of Poly 3-hexylthiophene in Oxidized and Unoxidized States. *J. Raman. Spectrosc.* **1998**, *29*, 825−832.
(42) Gao, J.; Stein, B. W.; Thomas, A. K.; Garcia, J. A.; Yang, J.; Kirk, M. L.; Grey, J. K. Enhanced Charge Transfer Doping Efficiency in J-Aggregate Poly(3-Hexylthiophene) Nanofibers. *J. Phys. Chem. C* **2015**, *119*, 16396−16402.
(43) Mansour, A. E.; Valencia, A. M.; Lungwitz, D.; Wegner, B.; Tanaka, N.; Shoji, Y.; Fukushima, T.; Opitz, A.; Cocchi, C.; Koch, N. Understanding the Evolution of the Raman Spectra of Molecularly P-Doped Poly(3-Hexylthiophene-2,5-Diyl): Signatures of Polarons and Bipolarons. *Phys. Chem. Chem. Phys.* **2022**, *24*, 3109−3118.
(44) Yamamoto, J.; Furukawa, Y. Electronic and Vibrational Spectra of Positive Polarons and Bipolarons in Regioregular Poly(3-Hexylthiophene) Doped with Ferric Chloride. *J. Phys. Chem. B* **2015**, *119*, 4788−4794.
(45) Sweetnam, S.; Graham, K. R.; Ngongang Ndjawa, G. O.; Heumüller, T.; Bartelt, J. A.; Burke, T. M.; Li, W.; You, W.; Amassian, A.; McGehee, M. D. Characterization of the Polymer Energy Landscape in Polymer:Fullerene Bulk Heterojunctions with Pure and Mixed Phases. *J. Am. Chem. Soc.* **2014**, *136*, 14078−14088.
(46) Bard, A. J.; Faulkner, L. R. Electroactive Layers and Modified Electrodes. In *Electrochemical Methods: Fundamentals and Applications*, 2nd ed.; John Wiley & Sons, 2001, pp 580−624.
(47) Amatore, C.; Savéant, J. M.; Tessier, D. Charge Transfer at Partially Blocked Surfaces. A Model for the Case of Microscopic Active and Inactive Sites. *J. Electroanal. Chem.* **1983**, *147*, 39−51.
(48) Le, T. H.; Kim, Y.; Yoon, H. Electrical and Electrochemical Properties of Conducting Polymers. *Polymers* **2017**, *9*, 150.
(49) Hernández-Ferrer, J.; Ansón-Casaos, A.; Martínez, M. T. Electrochemical Synthesis and Characterization of Single-Walled Carbon Nanotubes/Polypyrrole Films on Transparent Substrates. *Electrochim. Acta* **2012**, *64*, 1−9.
(50) Enengl, C.; Enengl, S.; Pluczyk, S.; Havlicek, M.; Lapkowski, M.; Neugebauer, H.; Ehrenfreund, E. Doping-Induced Absorption Bands in P3HT: Polarons and Bipolarons. *ChemPhysChem* **2016**, *17*, 3836−3844.
(51) Moreira, T.; Laia, C. A. T.; Zangoli, M.; Antunes, M.; Di Maria, F.; De Monte, S.; Liscio, F.; Parola, A. J.; Barbarella, G. Semicrystalline Polythiophene-Based Nanoparticles Deposited from Water on Flexible PET/ITO Substrates as a Sustainable Approach toward Long-Lasting Solid-State Electrochromic Devices. *ACS Appl. Polym. Mater.* **2020**, *2*, 3301−3309.
(52) Padilla, J.; Seshadri, V.; Sotzing, G. A.; Otero, T. F. Maximum Contrast from an Electrochromic Material. *Electrochem. Commun* **2007**, *9*, 1931−1935.
(53) Padilla, J.; Österholm, A. M.; Dyer, A. L.; Reynolds, J. R. Process Controlled Performance for Soluble Electrochromic Polymers. *Sol. Energy Mater. Sol. Cells* **2015**, *140*, 54−60.
(54) Kim, T. H.; Choi, K. I.; Kim, H.; Oh, S. H.; Koo, J.; Nah, Y. C. Long-Term Cyclability of Electrochromic Poly(3-Hexyl Thiophene) Films Modified by Surfactant-Assisted Graphene Oxide Layers. *ACS. Appl. Mater. Interfaces* **2017**, *9*, 20223−20230.
(55) Bargigia, I.; Savagian, L. R.; Österholm, A. M.; Reynolds, J. R.; Silva, C. Charge-Transfer Intermediates in the Electrochemical Doping Mechanism of Conjugated Polymers. *J. Am. Chem. Soc.* **2021**, *143*, 294−308.
(56) Nicolini, T.; Marquez, A. V.; Goudeau, B.; Kuhn, A.; Salinas, G. In Situ Spectroelectrochemical-Conductance Measurements as an Efficient Tool for the Evaluation of Charge Trapping in Conducting Polymers. *J. Phys. Chem. Lett.* **2021**, *12*, 10422−10428.

https://doi.org/10.1021/acs.chemmater.3c00008
Chem. Mater. 2023, 35, 3522−3531